ELSEVIER

Catalysis Today 68 (2001) 63–68

CATALYSIS TODAY

www.elsevier.com/locate/cattod

Nanosized metal oxides in the mesopores of MCM-41 and MCM-48 silicates

S.E. Dapurkar, S.K. Badamali, P. Selvam*

Department of Chemistry, Indian Institute of Technology – Bombay, Powai, Mumbai 400 076, India

This paper is dedicated to Prof. B. Viswanathan on the occasion of his 60th birthday

Abstract

The present work describes the preparation and characterization of nanosized metal oxide particles (Fe_2O_3, ZnO and PbO) inside the mesopore channels of MCM-41 and MCM-48 silicate molecular sieves. The encapsulation of the metal oxides was carried out at room temperature by the incipient wetness method. Diffuse reflectance ultraviolet–visible spectroscopic studies showed a significant shift in the absorption band for the entrapped metal oxides as compared to the corresponding bulk oxides. Thus, confirming the quantum confinement of the incorporated nanoparticles in MCM-41 and MCM-48.

Keywords: Nanosized metal oxides; Mesoporous materials; MCM-41; MCM-48; Host–guest chemistry

1. Introduction

Materials of nanometer scale is of considerable importance in the development of advanced quantum-confined electronic and optoelectronic devices such as lasers, switches, transistors and information storage processes [1]. Traditionally, colloidal solutions [2], porous glasses [3] and certain polymers [4] have been used as hosts for the preparation of nanosized materials. However, they are neither efficient in generating clusters of uniform size nor chemically inert towards the guest molecules. On the other hand, it was realized that the preparation of nanosized materials in zeolitic pores has several advantages and hence they have been considered to form ideal host systems [5,6]. Indeed, the regular pore structure of zeolite molecular sieves offers a suitable reaction chamber for the controlled assembling of nanostructured materials [7–11]. However, the smaller pore size of these materials limits their applicability. On the other hand, the recent discovery of mesoporous molecular sieves designated as M41S [12,13] have broadened the scope of applications. Two of the stable members of the M41S family, viz., hexagonal MCM-41 having unidimensional pore structure and cubic MCM-48 with three-dimensional pore system can comfortably trap the guest molecules in the mesopores [14–19,34]. Further, the well-defined pore size, large internal surface area associated with the open framework of the mesophases show promise for such purpose. Therefore, in the present investigation both MCM-41 and MCM-48 were used as host materials, and three binary metal oxides, viz., Fe_2O_3, ZnO and PbO, were selected as the guest molecules.

* Corresponding author. Fax: +91-22-572-3480.
E-mail address: selvam@iitb.ac.in (P. Selvam).

0920-5861/01/$ – see front matter
PII: S0920-5861(01)00323-6

2. Experimental

2.1. Starting materials

The following materials were used for the preparation of the mesoporous MCM-41 and MCM-48 silicates: fumed silica (99.8%, Aldrich), tetraethyl orthosilicate (TEOS; Aldrich, 98%), tetramethylammonium hydroxide (TMAOH; Aldrich, 25 wt.%), cetyltrimethylammonium bromide (CTAB; Aldrich, 99%), sodium hydroxide (NaOH; Loba, 98%), and distilled water. High purity metal nitrates, viz., $Fe(NO_3)_3{\cdot}9H_2O$ (>98%, Alfa), $Pb(NO_3)_2$ (>99.5%, Loba), and $Zn(NO_3)_2{\cdot}6H_2O$ (>98%, SDS) were used for loading. The bulk metal oxides, viz., Fe_2O_3 (99%, Merck), ZnO (>99%, Merck), and red PbO (>99%, Fluka) were employed as the standards for a comparative study. All the chemicals used in the present investigation were in the as-received forms without any further purification. However, the bulk metal hydroxides were freshly precipitated from the respective nitrate sources as per the procedure described elsewhere [20,35].

2.2. Synthesis of MCM-41 and MCM-48

The siliceous MCM-41 and MCM-48 were synthesized hydrothermally according to a procedure outlined earlier [20,21,35] in a Teflon-lined stainless steel autoclaves at 373 K for 24 h (MCM-41) and 72 h (MCM-48). The typical gel (molar) composition were $10SiO_2{:}1.35(CTA)_2O{:}0.75(TMA)_2O{:}1.3Na_2O{:}680H_2O$ and $SiO_2{:}0.3(CTA)_2O{:}0.25Na_2O{:}60H_2O$ for MCM-41 and MCM-48, respectively. The as-synthesized samples were calcined at 823 K in a flow of N_2, for an hour followed by 6 h in air, and were used as host materials for the inclusion of various guest metal hydroxides/oxides.

2.3. Loading of metal hydroxides/oxy-hydroxides/oxides

Incipient wetness method was employed for the inclusion of various metal ions under consideration in the host materials MCM-41 and MCM-48. Prior to loading, the samples were activated at 393 K. First, aqueous solutions of the respective metal nitrates (8×10^{-3} M) was added dropwise to 1 g of the mesoporous host and was kept under mild stirring for 2–3 h. It was then allowed to stand for 4–5 h in order to ensure maximum possible loading. The resulting products were repeatedly washed with distilled water and dried at room temperature followed by heating at 353 K for 8 h. These samples are designed as loaded metal oxy-hydroxide in MCM-41 and MCM-48. All the samples were calcined in air for 8 h in the temperature range 673–773 K in order to ensure the formation of corresponding metal oxides. These samples are referred to as loaded metal oxides in MCM-41 and MCM-48.

2.4. Characterization

Powder X-ray diffraction (XRD) patterns were recorded in the low angle region on Rigaku/Siemens diffractometers using a nickel filtered Cu Kα radiation ($\lambda = 1.5418$ Å) with a step size of 0.02°. Thermogravimetery (TG) measurements were carried out on a DuPont thermal analyzer (9900/2100) under nitrogen atmosphere. The surface area was measured by nitrogen adsorption–desorption method using a Smartsorb 90 equipment at liquid nitrogen temperature. Diffuse reflectance ultraviolet–visible (DRUV–Vis) spectra of the samples were recorded on an UV-260 Shimazdu spectrophotometer. The metal ion content of the loaded samples were determined (0.6–0.9 wt.%) by inductively coupled plasma-atomic emission spectroscopy (ICP-AES) on a Labtam Plasm Lab 8440 equipment.

3. Results and discussion

Figs. 1 and 2 show the typical XRD patterns of MCM-41 and MCM-48, respectively [12,13]. BET surface area ($1000\,m^2\,g^{-1}$ for MCM-41 and $1120\,m^2\,g^{-1}$ for MCM-48) as well as the TG weight loss (39% for MCM-41 and 58% for MCM-48) data indicate the mesoporous nature of the host materials. Fig. 3 depicts the XRD of FeO(OH)/MCM-48 and Fe_2O_3/MCM-48 samples and the patterns are characteristic of MCM-48 indicating the intactness of the structure upon loading and subsequent treatments. However, a decrease in peak intensities as compared to unloaded MCM-48 was noticed which can be attributed to increased contrast matching between

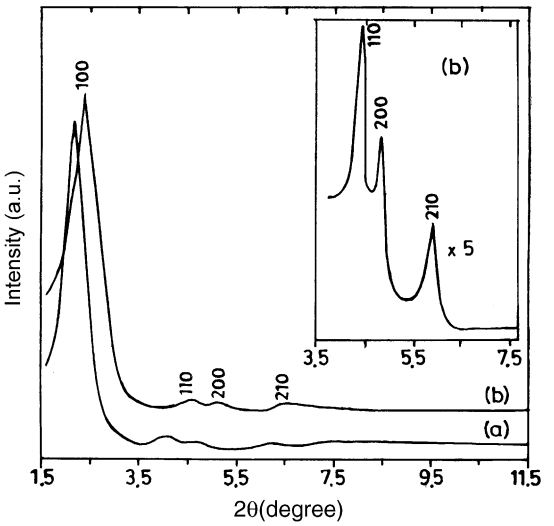

Fig. 1. XRD patterns of MCM-41: (a) as-synthesized; (b) calcined.

the silicate framework and the iron hydroxide/oxide nanoparticles present in the pore [17]. No additional peaks are observed at higher angle indicating that no crystalline metal oxide phase (bulk oxide) has been formed outside the pore structure. In fact, Abe et al. [14,34] have also confirmed earlier the presence of iron oxide nanoparticles in the pores of MCM-41 by platinum loading on iron oxide particles by photodeposition technique. Indeed, Fröba et al. [17] and Zhang et al. [22] have shown earlier by transmission electron microscopy that the particle size of the incorporated Fe_2O_3 in the mesopores of MCM-48 and ZnO nanoclusters in MCM-41 is smaller than the pore diameter.

Fig. 4 shows the DRUV–Vis spectra of FeO(OH)/MCM-41 and FeO(OH)/MCM-48 as well as Fe_2O_3/MCM-41 and Fe_2O_3/MCM-48 samples. For a comparison, the spectra of the bulk FeO(OH) and Fe_2O_3 as well as calcined FeO(OH) samples were included. As expected, the siliceous MCM-41 and MCM-48 show little or no absorbance in the range 200–700 nm. On the other hand, the bulk samples (see Fig. 4g–i) of freshly precipitated FeO(OH), calcined FeO(OH) and Fe_2O_3 all show broad bands with strong maxima at 535, 515 and 560 nm, respectively, arising from all possible d–d transitions [14,34]. On the other hand, the absorption maxima for colloidal α-Fe_2O_3 particles was reported to be 530 nm [23]. In contrast, the loaded samples show absorption bands at 250 nm (Fig. 4b–e).

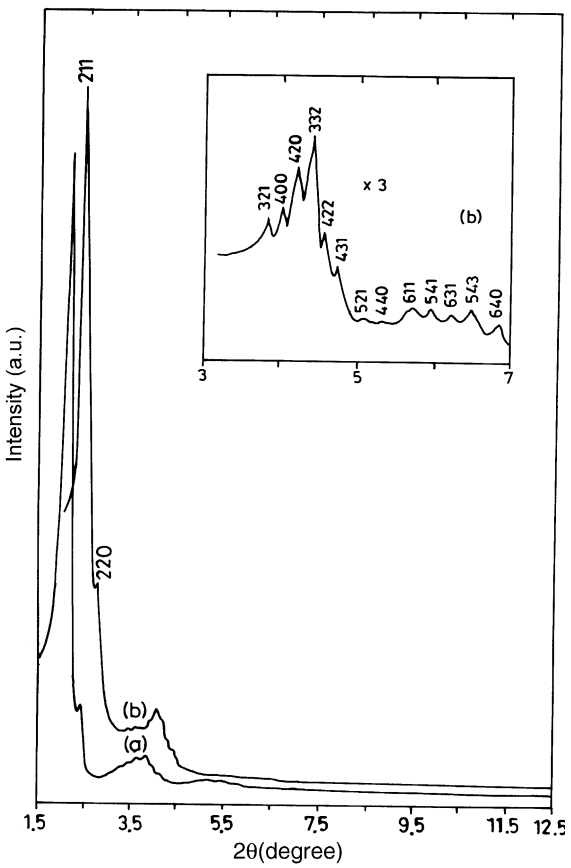

Fig. 2. XRD patterns of MCM-48: (a) as-synthesized; (b) calcined.

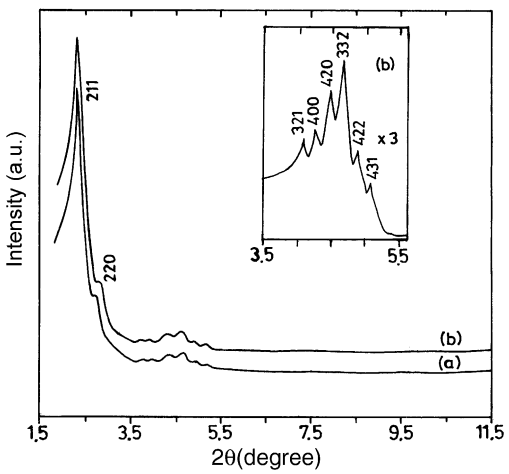

Fig. 3. XRD patterns of: (a) FeO(OH)/MCM-48; (b) Fe_2O_3/MCM-48.

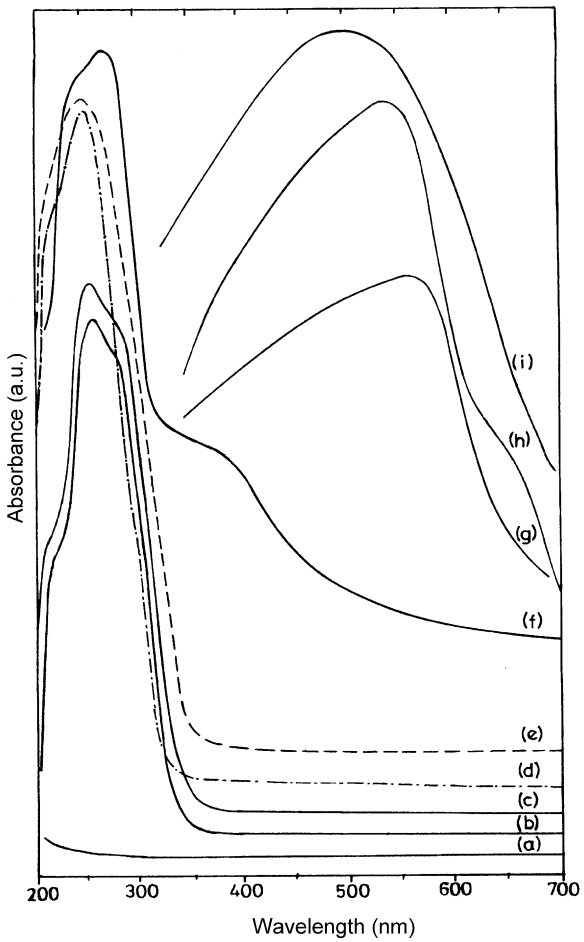

Fig. 4. DRUV–Vis spectra of: (a) calcined MCM-41/MCM-48; (b) FeO(OH)/MCM-41; (c) FeO(OH)/MCM-48; (d) Fe_2O_3/MCM-41; (e) Fe_2O_3/MCM-48; (f) Fe_2O_3/MCM-41 (0.01 M $Fe(NO_3)_3{\cdot}9H_2O$); (g) Fe_2O_3; (h) FeO(OH); (i) calcined FeO(OH).

The significant shift in the absorption bands is attributed to the encapsulation of FeO(OH)/Fe_2O_3 nanoparticles inside the mesopores. In fact, such a large (blue) shift in the absorption maxima of bulk Fe_2O_3 or α-Fe_2O_3 colloidal (560/530–250 nm) is associated with the transition in the particle size from bulk to the molecular order, viz., the quantum size effect [14,24–27,34]. It is interesting to note that no bulk Fe_2O_3 particles existed on the outer surface of MCM-41 and MCM-48 unless and otherwise the concentration of metal ion is increased to or higher than 0.01 M. For example, the absorption spectra of Fe_2O_3 in MCM-41 prepared with 0.01 M iron nitrate concentration gave a strong absorption in the range 350–550 nm in addition to a weak band at 250 nm (Fig. 4f). The strong band in the range 350–550 nm is attributed to the transition in the bulk Fe_2O_3 particles on the outer surface of MCM-41, while the band at 250 nm can be assigned to that the iron oxide nanoparticles in the mesopores [14,34]. Similar trends were observed for ZnO and PbO nanoparticles in MCM-41 and MCM-48.

DRUV–Vis spectra of various zinc samples are depicted in Fig. 5. As before, all the loaded samples show a maxima at ~260 nm (Fig. 5a–d). However, the bulk $Zn(OH)_2$ and ZnO samples appear in the range ~360–370 nm (Figs. 5e and 5g). Colloidal ZnO also shows an absorption band at 370 nm [28]. Again, the shift in the absorption maxima between the bulk or colloidal zinc oxide and loaded samples supports the encapsulation of $Zn(OH)_2$/ZnO particles in the mesopores of MCM-41 and MCM-48. The results are in agreement with the nanosized ZnO embedded

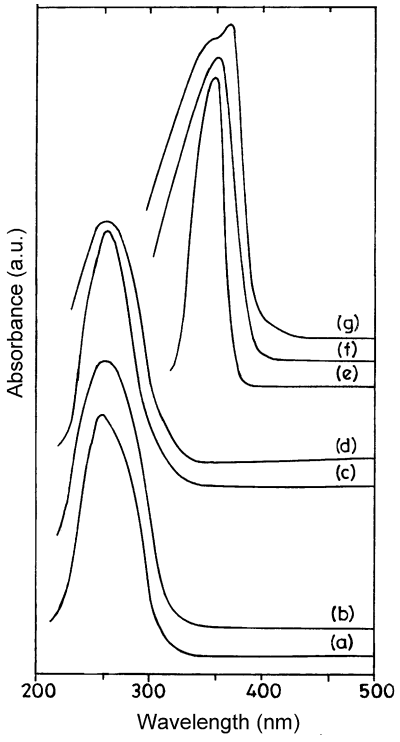

Fig. 5. DRUV–Vis spectra of: (a) $Zn(OH)_2$/MCM-41; (b) $Zn(OH)_2$/MCM-48; (c) ZnO/MCM-41; (d) ZnO/MCM-48; (e) calcined $Zn(OH)_2$; (f) ZnO; (g) $Fe(OH)_2$.

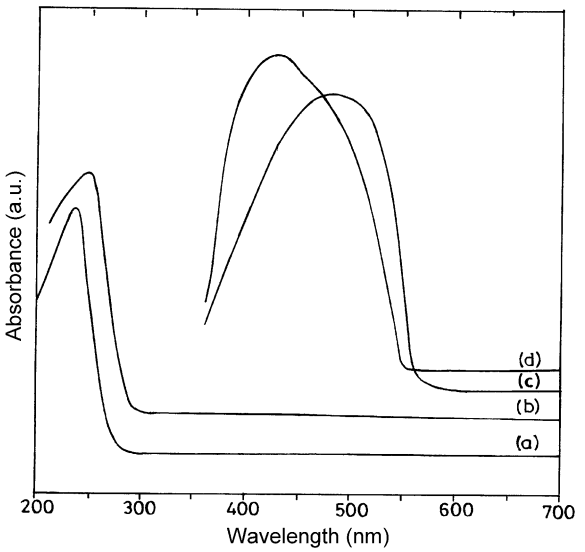

Fig. 6. DRUV–Vis spectra of: (a) PbO/MCM-41; (b) PbO/MCM-48; (c) red PbO; (d) precipitated (red) PbO.

in zeolite-A and MCM-41 [22,29,30]. Fig. 6 shows the DRUV–Vis spectra of the various lead samples. The loaded PbO samples show strong maxima in the region 245–255 nm (Fig. 6a and b). The reference samples, viz., red PbO (Fig. 6c) and precipitated (red) PbO (Fig. 6d) exhibit broad bands at 425 and 480 nm, respectively. A similar shift in absorption band and bandwidth observed in lead loaded samples as compared to colloidal lead particles. Once again, the observed shift from higher to lower wavelength could be attributed to the quantum size effect. A similar observation was noted earlier for PbS nanoclusters encapsulated in certain zeolites [9,31–33]. Fig. 7 illustrates a schematic representation of the formation of the various nanosized metal oxides assembled in the mesopores of MCM-41 and MCM-48.

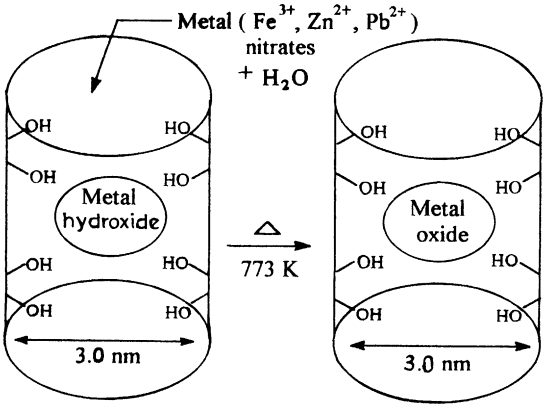

Fig. 7. A schematic representation of the encapsulation of nanosized metal oxides inside the mesoporous channels of MCM-41 and MCM-48 silicates molecular sieves.

4. Conclusion

In the present investigation, we have demonstrated the encapsulation of various nanosized metal oxides in the mesopore channels of MCM-41 and MCM-48. Interestingly, the absorption maxima appeared almost in the wavelength region (250–260 nm) irrespective of the encapsulated metal ions. It is therefore deduced that the observed (blue) shift in the absorption edge is as a consequence of the quantum size effect. It is also to be noted here that the absorption band for the isomorphously substituted metal ions in the mesoporous framework, e.g. FeMCM-41, also appears nearly in the same region as that of the incorporated nanoparticles, viz., Fe_2O_3/MCM-41 thus complicating the spectral analysis. Therefore, due care must be adopted while interpreting the DRUV–Vis data of the nanoparticles in mesoporous materials.

Acknowledgements

We thank Dr. P. Ayyub and Mr. Nilesh Kulkarni (TIFR, Mumbai) and Dr. K. Selvamuthupillai (ETH, Zürich) for XRD data.

References

[1] G. Schulz-Ekloff, Stud. Surf. Sci. Catal. 69 (1991) 65.
[2] R. Rossetti, R. Hall, J.M. Gibson, L.E. Brus, J. Chem. Phys. 83 (1985) 1406.
[3] A.I. Ekimov, Al.L. Efros, A.A. Onushcenko, Solid State Commun. 56 (1985) 921.
[4] E. Dalas, J. Kallitsis, S. Sakkopoulos, E. Vitoratos, P.G. Koutsoukos, J. Colloid Interf. Sci. 141 (1991) 137.
[5] G. Telbiz, A. Shwets, V. Gunko, J. Stoch, G. Tamulajtis, N. Kukhtarev, Stud. Surf. Sci. Catal. 84 (1994) 1099.
[6] G.D. Stucky, J.E. MacDougall, Science 247 (1990) 669.
[7] P. Behrens, G.D. Stucky, Angew. Chem. Int. Ed. Engl. 32 (1992) 696.

[8] Y. Nozue, in: T. Ogawa, K. Kanemitsu (Eds.), Optical Properties of Low-dimensional Materials, World Scientific, Singapore, 1995, p. 387.
[9] Y. Wang, N. Herron, J. Phys. Chem. 91 (1987) 257.
[10] N. Herron, Y. Wang, M.E. Eddy, G.D. Stucky, D.E. Cox, K. Moller, T. Bein, J. Am. Chem. Soc. 111 (1989) 530.
[11] G.A. Ozin, C. Gil, Chem. Rev. 89 (1989) 1749.
[12] C.T. Kresge, M.E. Leonowicz, W.T. Roth, J.C. Vartuli, J.S. Beck, Nature 359 (1992) 710.
[13] J.S. Beck, J.C. Vartuli, W.J. Roth, M.E. Leonowicz, K.D. Schmidtt, C.T.-W. Chu, D.H. Olson, E.W. Sheppard, S.B. McCullen, J.B. Higgins, J.L. Schlenker, J. Am. Chem. Soc. 114 (1992) 10834.
[14] T. Abe, Y. Tachibana, T. Uematsu, M. Iwamoto, J. Chem. Soc., Chem. Commun. (1995) 1617.
[15] X.S. Zhao, G.Q. Max Lu, G.J. Millar, Ind. Eng. Chem. Res. 35 (1996) 2075.
[16] K. Moller, T. Bein, Chem. Mater. 10 (1998) 2950.
[17] M. Fröba, R. Kohn, G. Bouffaud, Chem. Mater. 11 (1999) 2858.
[18] J.-S. Jung, W.-S. Chae, R.A. Mcintyre, C.T. Seip, J.B. Wiley, C.J. O'Connor, Mater. Res. Bull. 34 (1999) 1353.
[19] T. Hirai, H. Okubo, I. Komasawa, J. Phys. Chem. 103 (1999) 4228.
[20] S.K. Badamali, P. Selvam, Stud. Surf. Sci. Catal. 113 (1998) 749.
[21] R. Schmidt, M. Stocker, D. Akporiaye, E.H. Torstad, A. Olsen, Microporous Mater. 5 (1995) 1.
[22] W.-H. Zhang, J.-L. Shi, L.-Z. Wang, D.-S. Yan, Chem. Mater. 12 (2000) 1408.
[23] J. Kiwi, M. Gratzel, J. Chem. Soc., Faraday Trans. 83 (1987) 1101.
[24] L. Brus, J. Phys. Chem. 90 (1986) 2555.
[25] A.P. Alivisatos, Science 271 (1996) 933.
[26] J.Z. Zhang, Acc. Chem. Res. 30 (1997) 423.
[27] H. Miyoshi, H. Yoneyama, J. Chem. Soc., Faraday Trans. 85 (1989) 1873.
[28] D.W. Bahnemann, C. Kormann, M.R. Hoffmann, J. Phys. Chem. 91 (1987) 3789.
[29] A. Fojtik, H. Weller, U. Koch, A. Henglein, Ber. Bunsen-Ges. Phys. Chem. 88 (1984) 969.
[30] M. Haase, A. Henglein, J. Phys. Chem. 92 (1988) 482.
[31] T. Turk, F. Sabin, A. Vogler, Mater. Res. Bull. 27 (1992) 1003.
[32] K. Moller, T. Bein, N. Herren, W. Mahler, Y. Wang, Inorg. Chem. 28 (1989) 2914.
[33] M. Wark, G. Schulz-Ekloff, N.I. Jaeger, Catal. Today 8 (1991) 467.
[34] M. Iwamoto, T. Abe, Y. Tachibana, J. Mol. Catal. A 155 (2000) 143.
[35] S.K. Badamali, Ph.D. Thesis, IIT Bombay, Mumbai, 1999.